日本原子力研究開発機構機関リポジトリ

Japan Atomic Energy Agency Institutional Repository

Title	Spinmotive force in the out-of-plane direction generated by spin wave excitations in an exchange-coupled bilayer element
Author(s)	Zhou W., Seki Takeshi, Imamura Hiroshi, Ieda Junichi, Takanashi Koki
Citation	Physical Review B,100(9),p.094424_1-094424_5
Text Version	Published Journal Article
URL	https://jopss.jaea.go.jp/search/servlet/search?5066089
DOI	https://doi.org/10.1103/PhysRevB.100.094424
Right	©2019 American Physical Society

Japan Atomic Energy Agency

Spinmotive force in the out-of-plane direction generated by spin wave excitations in an exchange-coupled bilayer element

W. Zhou[1,*] T. Seki,[1,2,†] H. Imamura,[3] J. Ieda[4] and K. Takanashi[1,2]

[1]*Institute for Materials Research, Tohoku University, Sendai 980-8577, Japan*
[2]*Center for Spintronics Research Network, Tohoku University, Sendai 980-8577, Japan*
[3]*National Institute of Advanced Industrial Science and Technology, Spintronics Research Center, Tsukuba 305-8568, Japan*
[4]*Advanced Science Research Center, Japan Atomic Energy Agency, Tokai 319-1195, Japan*

The generation of the spinmotive force (SMF) requires the temporal and spatial variations of the magnetic moments. We explore an approach to satisfy this requirement by creating asymmetry in a thin film structure along the out-of-plane direction, through the use of an exchange-coupled $L1_0$-FePt/$Ni_{81}Fe_{19}$ bilayer element. As the spin wave is excited by a rf magnetic field, a continuous dc voltage signal in the out-of-plane direction of the bilayer element appears. The sign of the voltage signal and its microwave power dependency agree with the theoretical framework of the SMF. The corresponding spin wave modes are revealed by carrying out the micromagnetic simulation. Our results demonstrate the generation of the SMF using a vertically structured element in addition to previously reported in-plane structured devices.

DOI: 10.1103/PhysRevB.100.094424

I. INTRODUCTION

The transfer of spin angular momentum from the conduction electron to the local magnetic moment, i.e., the spin-transfer torque (STT) [1,2], has been proven to be a powerful tool to manipulate magnetic moments and induce magnetization dynamics, demonstrating the potential of high performance in spintronics devices, such as magnetic random access memories and spin-torque oscillators [3–5]. On the other hand, the reciprocal process of the STT has been less explored for such device applications. Usually termed the spinmotive force (SMF), this effect has been the subject of theoretical study for decades [6–16], indicating that the temporal and spatial variations of the local magnetic moments generate an electrical voltage. The SMF can be expressed by the spin-electric field,

$$E_s = \frac{P\hbar}{2e} \boldsymbol{m} \cdot (\partial_t \boldsymbol{m} \times \nabla \boldsymbol{m}), \tag{1}$$

where P is the spin polarization of the conduction electron, $\hbar$ is the reduced Planck constant, e is the elementary charge, and $\boldsymbol{m}$ is the unit vector representing the direction of the local magnetic moment. As exhibited in the bracket on the right-hand side of Eq. (1), the generation of the SMF requires that $\boldsymbol{m}$ depends both on time and space. It can be experimentally realized by exciting the magnetization dynamics of a nonuniform magnetic texture. However, this demands creating and controlling such magnetic textures, which usually have the length scale of submicrometers. The difficulty of doing so

may be a reason for the SMF not being experimentally observed until recent years. One of the well-studied nonuniform magnetic textures is a domain wall in a magnetic nanowire, and it was used for the first experimental observation of the SMF by moving the domain wall and capturing the small voltage signal with a modulation technique [17,18]. A later experiment using real-time voltage measurement further verified the sign of the SMF being consistent with theory, and showed that the SMF does not depend on the speed of the domain wall motion, but scales with the magnetic field (H) driving the motion [19]. Recent numerical studies suggested that the SMF due to the domain-wall motion can be enhanced or altered by changing the shape of the nanowire [20,21] or exploiting the Dzyaloshinskii-Moriya interaction [22]. Meanwhile, the SMF was also experimentally observed by exciting the magnetization dynamics in other nonuniform magnetic textures, which were created by controlling the shape of the lithographically patterned magnetic thin films, such as a magnetic vortex structure [23], a comb-shaped element [24], or a wedged wire [25]. The SMF generation using the skyrmion lattice [26] or the magnetic bubble [27] has also been studied by simulation, suggesting the potential of the SMF as a tool to study and explore the dynamics of magnetic texture. Although the SMF generation was observed using the nonuniform magnetic textures in the plane of the thin film, no detailed examination of the SMF has been carried out exploiting the nonuniformity in the out-of-plane direction. Such a vertically structured element is an area of research interest in multilayer thin films, which have become a building block for recent spintronic devices. Therefore, it is of importance to understand the SMF generation from the nonuniform magnetic textures in the *out-of-plane* direction.

In this paper, we experimentally explore an approach for the generation of the SMF using the out-of-plane nonuniform

---

*Present address: Research Center for Magnetic and Spintronic Materials, National Institute for Materials Science, Tsukuba 305-0047, Japan; zhou.weinan@nims.go.jp
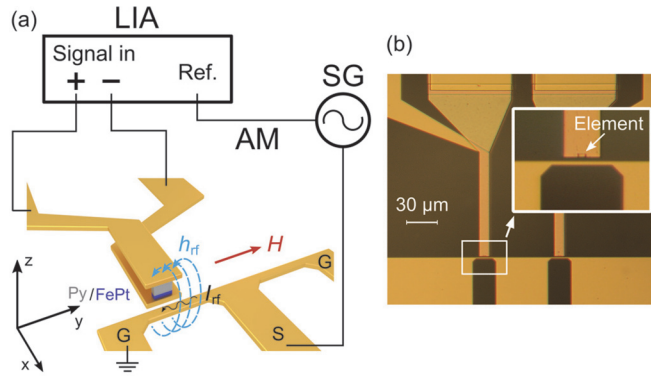†go-sai@imr.tohoku.ac.jp

FIG. 1. (a) Schematic illustration of the device structure and measurement setup. The reference signal of the lock-in amplifier (LIA) is fed into the signal generator (SG) for amplitude modulation (AM). I_{rf} passes through the short end of the coplanar waveguide (CPW) and generates h_{rf} to excite the spin wave in the $L1_0$-FePt/Py bilayer element. The red arrow indicates the direction of H, which is aligned to the y axis. The voltage signal between the top and bottom of the bilayer element is captured by LIA. (b) Microscopic image of the device. Two bilayer elements in two separate measurement circuits with the top and bottom electrodes are placed at the top of the image, facing the short end of the CPW. Magnification of a bilayer element is shown in the inset of (b).

magnetic texture created by asymmetry in a layered structure, i.e., an exchange-coupled bilayer consisting of a hard magnetic $L1_0$-FePt layer and a soft magnetic $Ni_{81}Fe_{19}$ (Permalloy; Py) layer. Such a bilayer structure has previously demonstrated the excitation of perpendicular standing spin wave (PSSW) modes [28–30]. In this study, we focus on the situation where the magnetization of both the FePt and Py layers are aligned to H. The FePt layer has in-plane uniaxial magnetic anisotropy, and pins the magnetic moments at one end of the bilayer element. As the spin wave is excited by a rf magnetic field (h_{rf}) application, the temporal and spatial variations of magnetic moments are produced, which leads to a continuous electrical voltage in the out-of-plane direction of the bilayer element. The micromagnetic simulation for the induced magnetization dynamics allows us to identify the spin wave mode responsible for the generation of the SMF. The sign of the voltage signal and its microwave power dependency are analyzed, which is in agreement with the theory of the SMF.

II. METHODS

A blanket thin film containing the exchange-coupled $L1_0$-FePt/Py bilayer was prepared on an MgO (110) single-crystal substrate. The stacking structure of the thin film was MgO (110) subs.//Cr (10)/Pt (10)/Au (40)/FePt (10)/Py (100)/Au (10) (thickness in nanometers). The composition of the FePt layer was determined to be $Fe_{48}Pt_{52}$ by the electron probe x-ray microanalysis. The preparation of the thin film has been described in detail in Ref. [31]. The epitaxially grown $L1_0$-FePt exhibited an in-plane uniaxial magnetic anisotropy along the MgO [001] direction, which is parallel to the y axis in Fig. 1(a). Then, the blanket thin film was microfabricated into the device shown in Fig. 1. The bottom electrode of the

measurement circuit was made by electron beam lithography and Ar ion milling, followed by the patterning of the bilayer element with the size of 2×0.4 μm^2. The long axis of the rectangular element is parallel to the MgO [001] direction. The milling process of the element was stopped when it reached the 40-nm-thick Au buffer layer by monitoring the secondary ion mass spectroscopy, and the remaining buffer layer was used as the bottom electrode. The surrounding of the element was filled by a 100-nm-thick AlO_x layer for insulation. Finally, the top surface of the element was exposed and cleaned, followed by deposition of Cr (3)/Au (50), which was patterned into the top electrode and the coplanar waveguide (CPW). This design allowed us to separate the measurement circuit consisting of the top and bottom electrodes and the bilayer element from the CPW, preventing the applied microwave power from passing directly through the element. However, there is still finite inductive coupling between the measurement circuit and the CPW. In order to minimize this effect, the top and bottom electrodes of the measurement circuit are designed to have the same width and similar thickness. The microscopic image of the device is shown in Fig. 1(b). The gap between the measurement circuit and the CPW was designed to be 1 μm, as well as the width of the short end of the CPW. The distance between the central line of the bilayer element and the edge of the top and bottom electrodes was designed to be 0.5 μm, resulting in a total 2 μm distance between the central line of the element and that of the short end. The element was magnetized by $H = 20$ kOe along the y axis prior to the measurement, in order to set the magnetization of the FePt layer. To reduce the noise and capture the small voltage signal, the lock-in amplifier (LIA) was used for measurement, and its reference signal was fed to the signal generator (SG) for amplitude modulation (AM) of the microwave power. The measurement setup is shown in Fig. 1(a). The modulated I_{rf} passing through the short end of the CPW generated h_{rf}. As a result, h_{rf} along the z axis was applied to the element for spin wave excitation [32]. H was applied along the y axis, while the generated voltage signal between the top and bottom of the element was captured by LIA.

Micromagnetic simulation was carried out in order to understand the spin wave excited in the bilayer element. We used the MUMAX3 package [33], and created the model of a cuboid with 400 nm along the x axis, 2000 nm along the y axis, and 110 nm along the z axis. The z axis corresponds to the thickness of the bilayer element, which consists of the 10-nm-thick FePt and 100-nm-thick Py layers. The bottom 10-nm-thick region along the z axis was for the FePt layer, and the material parameters for this layer were set as follows: the saturation magnetization (M_s) was 1.07×10^6 A/m, and the uniaxial magnetocrystalline anisotropy (K_u) was 1.1×10^6 J/m^3 along the y axis. These values were obtained from the experimentally measured hysteresis loop of the thin film. The top 100-nm-thick region along the z axis was for the Py layer with $M_s = 0.8 \times 10^6$ A/m and $K_u = 0$ J/m^3. We chose a stiffness constant of $A_{ex} = 1.3 \times 10^{-11}$ J/m for the whole system. No surface and interface anisotropies were taken into account. The model was divided into discrete computational cells, and the size of each cubic cell was $5 \times 5 \times 5$ nm^3. The damping parameters (α) of FePt and Py were set as 0.020
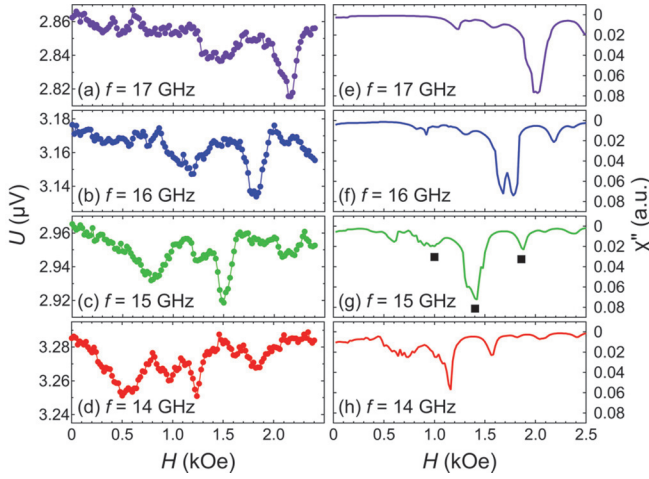
FIG. 2. (a) Experimentally measured U-H curves under the microwave power application of 20 dBm with $f = 17$, (b) 16, (c) 15, and (d) 14 GHz. (e) The ferromagnetic resonance (FMR) spectra of the bilayer element calculated by micromagnetic simulation under h_{rf} of 45 Oe with $f = 17$, (f) 16, (g) 15, and (h) 14 GHz. The vertical axes of (e)—(h) are inverted for comparison with the U-H curves. The black squares in (g) mark the conditions for the results shown in Fig. 3.

and 0.008, respectively [28]. The initial state was prepared by relaxing the uniformly magnetized state along the positive y axis. Then we applied h_{rf} with a certain amplitude and frequency (f) along the z axis. The excited magnetization dynamics were simulated for 10 ns plus two periods of h_{rf}. The imaginary part of the magnetic susceptibility (χ'') was obtained by fitting the spatial average of m_z during the last two periods of h_{rf} with the trigonometric functions. The snapshots of the magnetization dynamics were also captured in the last two periods of h_{rf}.

III. RESULTS AND DISCUSSION

In order to capture the voltage signal under the spin wave excitation, the constant microwave power was applied to the CPW while H was varied from 2.4 to 0 kOe. The dc voltage signal at $H = 0$ kOe was used to tune the phase of the lock-in detection to maximize the x component of the measured signal (U), and U as a function of H (U-H curves) under the microwave power application of 20 dBm with $f = 17$, 16, 15, and 14 GHz are shown in Figs. 2(a), 2(b), 2(c), and 2(d), respectively. Each U-H curve shown in this paper is an average of five measurements. Due to the inductive coupling, the microwave power applied to the CPW caused a background of several microvolts to the U-H curves. More importantly, there were dips in the voltage signal as H varied. The calculated ferromagnetic resonance (FMR) spectra of the bilayer element under h_{rf} of 45 Oe with $f = 17$, 16, 15, and 14 GHz are also shown in Fig. 2. The vertical axes of the FMR spectra are inverted for comparison with the U-H curves. The value of h_{rf} used in simulation was the estimated value based on the calculated I_{rf} in the short end of the CPW assuming impedance matching. The dips in the FMR spectra indicate the conditions of the excited spin wave modes. One
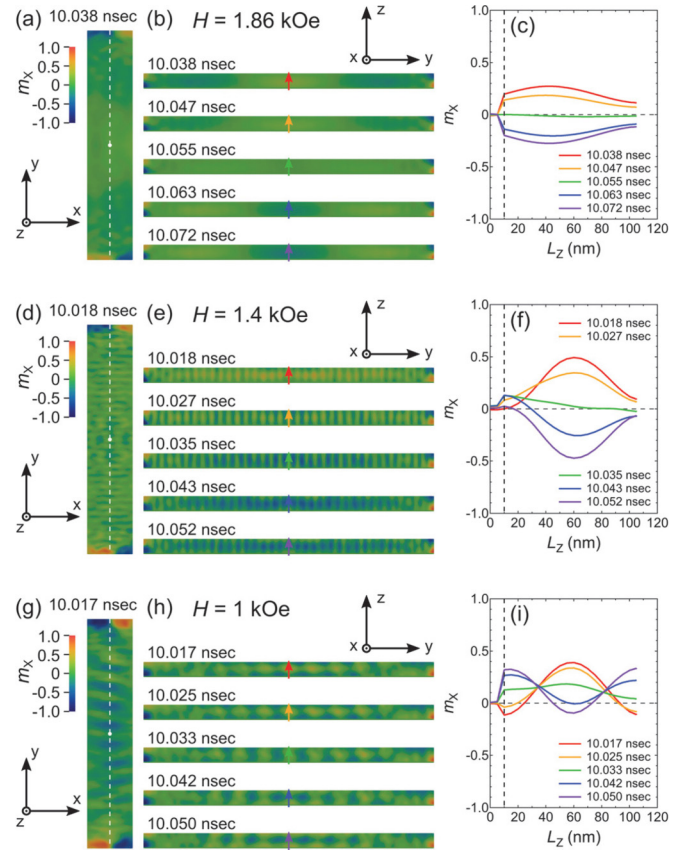

FIG. 3. (a) Snapshot of the top Py surface for m_x under $H = 1.86$ kOe along the y axis, and $h_{rf} = 45$ Oe along the z axis with $f = 15$ GHz. (b) Cross sections in the yz plane as indicated by the white dashed line in (a) evolve for half the period of h_{rf}. (c) Plots of m_x along the z axis at the center of the model [indicated by the white dot in (a) and colored arrows in (b)] for half the period of h_{rf}. The black dashed line indicates the interface between FePt and Py. (d) Snapshot of the top Py surface for m_x under $H = 1.4$ kOe. (e) Cross sections in the yz plane as indicated by the white dashed line in (d). (f) Plots of m_x along the z axis at the center of the model. (g) Snapshot of the top Py surface for m_x under $H = 1$ kOe. (h) Cross sections in the yz plane as indicated by the white dashed line in (g). (i) Plots of m_x along the z axis at the center of the model.

can see the clear correlation between the U-H curves and the FMR spectra, e.g., the ones with the largest magnitude [i.e., the dips at $H = 2.16$ kOe in Fig. 2(a) and at $H = 2$ kOe in Fig. 2(e)], as they shifted towards low H with decreasing f. It is worth noticing that the voltage signal due to the spin wave excitation is negative. This can be explained within the theoretical framework of the SMF, and will be discussed later.

The simulated magnetic structures under the stable spin wave excitation were used to understand the magnetization dynamics responsible for the measured voltage signals. The results under $H = 1.86$, 1.4, and 1 kOe along the y axis and h_{rf} along the z axis with $f = 15$ GHz are shown in Figs. 3(a)–3(c), 3(d)–3(f), and 3(g)–3(i), respectively. These conditions are also marked by the black squares shown in the FMR spectrum [Fig. 2(g)]. For $H = 1.86$ kOe, the results indicate that it is a PSSW mode with no nodes along the z axis ($n = 0$). The magnetic moments in FePt near the FePt/Py interface are

excited, and are oscillating in phase with the Py layer in this case, as shown in Fig. 3(c). For $H = 1.4$ kOe, the plot along the z axis [Fig. 3(f)] indicates that the magnetic moments in FePt near the FePt/Py interface are also excited, however, are lagging behind the dynamics of the Py layer. As a result, there is one node in the Py layer near the FePt/Py interface. The maximum value of m_x is larger than other modes shown here, with the largest χ'' in the FMR spectrum [Fig. 2(g)], which also corresponds to the dip with the largest magnitude shown in the U-H curve. The snapshots suggest that the element is divided into small areas ($\sim$30 nm) along the y axis due to the spin wave mode in the film plane. The results of $H = 1$ kOe indicate the excited spin wave mode is a PSSW mode with $n = 2$. Although the maximum value of m_x is large, it is canceled out partially by itself, and results in small χ'' in the FMR spectrum. The magnetization dynamics in the present exchange-coupled bilayer element resemble the case of FMR in the comb-shaped element [24], as the pinned magnetization at one end of the bilayer element can be considered as the part not in the FMR excitation. It is shown that the cone angle of the oscillating magnetic moments has a positive correlation with the SMF. For the PSSW mode with $n = 2$, the magnetic moments oscillating out of phase may generate the SMF of opposite sign along the z axis, which results in a small voltage signal between the top and bottom of the element. On the other hand, for the PSSW mode with $n = 0$, the magnetic moments in FePt near the FePt/Py interface oscillate in phase with the Py layer, and account for part of the temporal and spatial variation. Since the SMF is proportional to P as indicated by Eq. (1), the smaller P of FePt [34] compared to that of Py [19] may attribute to a small magnitude of the voltage signal. As a result, the PSSW mode with $n = 1$ exhibited the largest dip in the U-H curve.

The microwave power dependence of the voltage signal was also investigated. The U-H curves measured under the microwave power of 20 dBm (100 mW), 18 dBm (63 mW), and 15 dBm (32 mW) are shown in Figs. 4(a), 4(b), and 4(c), respectively. The calculated FMR spectra of the bilayer element under h_{rf} of 45, 35, and 25 Oe are also shown in Fig. 4 for comparison. For the experimentally measured U-H curves, the background decreases as the microwave power decreases. In addition, the dips of the voltage signals show a decrease in magnitude as the power decreases as well. The voltage signal of the dips (ΔU) in the U-H curves was extracted by subtracting the background voltage at $H = 0$ kOe, and plotted as a function of microwave power as shown in Fig. 4(g). The magnitude of ΔU is linearly proportional to the microwave power. This dependency is consistent with the SMF observed in the comb-shaped element [24], supporting our claim that the observed voltage signals originate from the SMF. Moreover, it is worth mentioning that ΔU reported here is in the same order compare to the SMF in the comb-shaped element [24] under the same microwave power, suggesting a similar efficiency of converting the dynamics of magnetic moments to dc voltage. On the other hand, one can see a small upward field shift of the dips of the voltage signals with increasing microwave power. This upward field shift is also observed in the calculated FMR spectra with increasing h_{rf} as shown in Figs. 4(d)–4(f). One possible explanation for this nonlinear effect is related to the amplitude of the
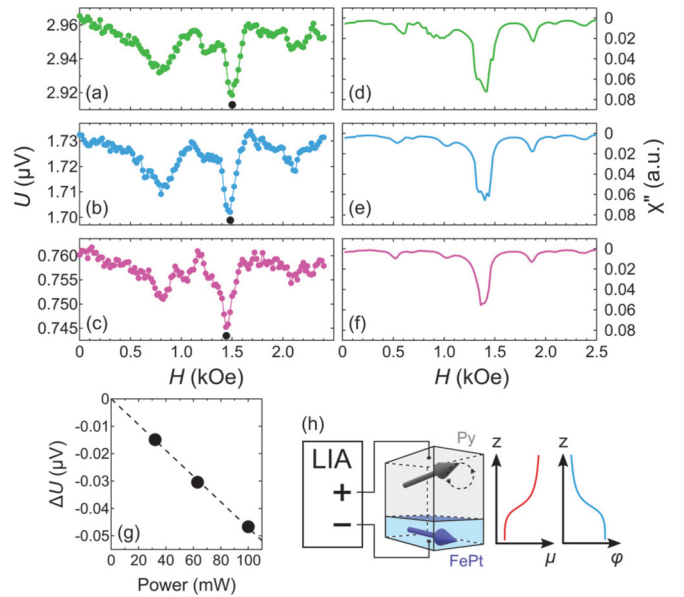

FIG. 4. (a) Experimentally measured U-H curves with $f = 15$ GHz and the microwave power of 20, (b) 18, and (c) 15 dBm. (d) The FMR spectra of the bilayer element calculated by micromagnetic simulation under h_{rf} of 45, (e) 35, and (f) 25 Oe with $f = 15$ GHz. The vertical axes of (d)–(f) are inverted for comparison with the U-H curves. (g) The microwave power dependence of ΔU at the dips indicated by the black circles in (a)–(c). The black dashed line is a linear fitting through the origin. (h) Schematic illustrations of the SMF generation and measurement in our setup, and the corresponding plots of electrochemical potential (μ) and electric potential (φ) along the z axis.

PSSW modes. The upward resonant field shift corresponds to a redshift of the resonant frequency. The increase in the amplitude of the PSSW modes with increasing h_{rf} suggests an increase in the cone angle of the magnetization precession for each magnetic moment. Such an increase in the cone angle often leads to the redshift of the resonant frequency [35].

The schematic illustrations in Fig. 4(h) are to show the negative sign of the SMF observed in this study. As the spin wave is excited in the bilayer element, the magnetic moments at the top Py surface are free to oscillate while the ones at the bottom FePt end are pinned. The temporal and spatial variations of the magnetic moments create a nonconservative spin force [10] acting on the electrons, which leads to an increase of electrochemical potential (μ) at the top Py surface, as indicated by the red curve. Due to the negative charge of electron, the electric potential $\varphi = \mu/(-e)$ at the top Py surface is lower than that at the bottom FePt end (blue curve). As a result, a negative voltage signal due to the SMF is captured by LIA. This situation can also be understood as an analogy to the SMF generated by the propagating domain wall in a magnetic nanowire. The bottom FePt end corresponds to the domain with magnetization parallel to H, while the top Py surface corresponds to the domain antiparallel to H. As the domain-wall motion is driven by H, the potential drop in φ due to the SMF develops toward the domain antiparallel to H [19].

The generation of the SMF using the vertically structured element has several advantages compared with that using the in-plane structured devices such as the domain-wall devices or the comb-shaped element. In the case of using the domain-wall motion, it is difficult to generate the continuous dc voltage signal, since the SMF disappears when the domain wall vanishes at the end of the magnetic nanowire. Considering this point, the utilization of spin wave excitation is suitable for the continuous dc voltage generation. In addition, it would be much more favorable to exploit the vertically structured element for the highly integrated spintronic devices compared with the in-plane structured devices.

IV. SUMMARY

The generation of the SMF using a nonuniform magnetic texture in the out-of-plane direction was explored, by exciting the spin wave in an exchange-coupled bilayer element consisting of a hard magnetic $L1_0$-FePt layer and a soft magnetic Py layer. The change in the voltage signal between the top and bottom of the bilayer element was measured as H was varied. The sign of the voltage signal as well as its microwave power dependency agreed with the theoretical framework of SMF. The FMR spectra obtained from micromagnetic simulation showed a correlation with the experimentally measured voltage signal, and exhibited the spin wave mode responsible for the signal. This paper demonstrated the generation of the SMF using a vertically structured element in addition to previously reported in-plane structured devices, and discussed the advantage of using the spin wave dynamics in the exchange-coupled bilayer element for the SMF generation.

[1] L. Berger, Phys. Rev. B **54**, 9353 (1996).

[2] J. C. Slonczewski, J. Magn. Magn. Mater. **159**, L1 (1996).

[3] D. Ralph and M. Stiles, J. Magn. Magn. Mater. **320**, 1190 (2008).

[4] A. Brataas, A. D. Kent, and H. Ohno, Nat. Mater. **11**, 372 (2012).

[5] N. Locatelli, V. Cros, and J. Grollier, Nat. Mater. **13**, 11 (2014).

[6] V. Korenman, J. L. Murray, and R. E. Prange, Phys. Rev. B **16**, 4032 (1977).

[7] L. Berger, Phys. Rev. B **33**, 1572 (1986).

[8] G. E. Volovik, J. Phys. C **20**, L83 (1987).

[9] A. Stern, Phys. Rev. Lett. **68**, 1022 (1992).

[10] S. E. Barnes and S. Maekawa, Phys. Rev. Lett. **98**, 246601 (2007).

[11] Y. Tserkovnyak and M. Mecklenburg, Phys. Rev. B **77**, 134407 (2008).

[12] M. Stamenova, T. N. Todorov, and S. Sanvito, Phys. Rev. B **77**, 054439 (2008).

[13] K.-W. Kim, J.-H. Moon, K.-J. Lee, and H.-W. Lee, Phys. Rev. Lett. **108**, 217202 (2012).

[14] H. Kawaguchi and G. Tatara, J. Phys. Soc. Jpn. **83**, 074710 (2014).

[15] K. M. D. Hals and A. Brataas, Phys. Rev. B **91**, 214401 (2015).

[16] C. S. Ho, M. B. A. Jalil, and S. G. Tan, New J. Phys. **17**, 123005 (2015).

[17] S. A. Yang, G. S. D. Beach, C. Knutson, D. Xiao, Q. Niu, M. Tsoi, and J. L. Erskine, Phys. Rev. Lett. **102**, 067201 (2009).

[18] S. A. Yang, G. S. D. Beach, C. Knutson, D. Xiao, Z. Zhang, M. Tsoi, Q. Niu, A. H. MacDonald, and J. L. Erskine, Phys. Rev. B **82**, 054410 (2010).

[19] M. Hayashi, J. Ieda, Y. Yamane, J.-I. Ohe, Y. K. Takahashi, S. Mitani, and S. Maekawa, Phys. Rev. Lett. **108**, 147202 (2012).

[20] Y. Yamane, J. Ieda, J. Ohe, S. E. Barnes, and S. Maekawa, Appl. Phys. Express **4**, 093003 (2011).

[21] J. Ieda and S. Maekawa, Appl. Phys. Lett. **101**, 252413 (2012).

[22] Y. Yamane, Phys. Rev. B **98**, 174434 (2018).

[23] K. Tanabe, D. Chiba, J. Ohe, S. Kasai, H. Kohno, S. E. Barnes, S. Maekawa, K. Kobayashi, and T. Ono, Nat. Commun. **3**, 845 (2012).

[24] Y. Yamane, K. Sasage, T. An, K. Harii, J. Ohe, J. Ieda, S. E. Barnes, E. Saitoh, and S. Maekawa, Phys. Rev. Lett. **107**, 236602 (2011).

[25] M. Nagata, T. Moriyama, K. Tanabe, K. Tanaka, D. Chiba, J. Ohe, Y. Hisamatsu, T. Niizeki, H. Yanagihara, E. Kita, and T. Ono, Appl. Phys. Express **8**, 123001 (2015).

[26] J. Ohe and Y. Shimada, Appl. Phys. Lett. **103**, 242403 (2013).

[27] Y. Yamane, S. Hemmatiyan, J. Ieda, S. Maekawa, and J. Sinova, Sci. Rep. **4**, 6901 (2014).

[28] T. Seki, K. Utsumiya, Y. Nozaki, H. Imamura, and K. Takanashi, Nat. Commun. **4**, 1726 (2013).

[29] T. Seki, W. Zhou, and K. Takanashi, J. Phys. D: Appl. Phys. **49**, 075002 (2016).

[30] W. Zhou, T. Seki, H. Arai, H. Imamura, and K. Takanashi, Phys. Rev. B **94**, 220401(R) (2016).

[31] W. Zhou, T. Yamaji, T. Seki, H. Imamura, and K. Takanashi, Appl. Phys. lett. **110**, 082401 (2017).

[32] M. V. Costache, S. M. Watts, M. Sladkov, C. H. van der Wal, and B. J. van Wees, Appl. Phys. Lett. **89**, 232115 (2006).

[33] A. Vansteenkiste, J. Leliaert, M. Dvornik, M. Helsen, F. Garcia-Sanchez, and B. V. Waeyenberge, AIP Adv. **4**, 107133 (2014).

[34] S. Mitani, K. Tsukamoto, T. Seki, T. Shima, and K. Takanashi, IEEE Trans. Magn. **41**, 2606 (2005).

[35] T. Moriyama, X. Fan, Y. Q. Wen, H. W. Zhang, and J. Q. Xiao, IEEE Trans. Magn. **45**, 2047 (2009).